Gas emissions at the continental margin west off Svalbard: Mapping, sampling, and quantification

H. Sahling[1], M. Römer[1], T. Pape[1], B. Bergès[2], C. dos Santos Fereirra[1], J. Boelmann[3, 4], P. Geprägs[1], M. Tomczyk[1], N. Nowald[1], W. Dimmler[5], L. Schroedter[1], M. Glockzin[6], and G. Bohrmann[1]

[1] {MARUM and Department of Geoscience, Klagenfurter Str, 28359 Bremen, Germany}

[2] {Institute of Sound and Vibration Research, University of Southampton, University Road, Southampton SO17 1BJ, United Kingdom}

[3] {Hochschule Bremerhaven, Labor für Maritime Technologien, An der Karlstadt 8, 27568 Bremerhaven, Germany}

[4] {Institute for Chemistry and Biology of the Marine Environment, University of Oldenburg, Carl-von-Ossietzky-Str. 9-11, 26111 Oldenburg, Germany}

[5] {FIELAX, Gesellschaft für wissenschaftliche Datenverarbeitung mbH, Schleusenstr. 14, 27568 Bremerhaven, Germany}

[6] {Institute of Baltic Sea Research, Warnemünde, Chemical Oceanography, Seestr. 15, 18119 Warnemünde, Germany}

Correspondence to: hsahling@marum.de

Abstract

We mapped, sampled, and quantified gas emissions at the continental margin west of Svalbard during R/V Heincke cruise He-387 in late summer 2012.

Hydroacoustic mapping revealed that gas emissions were not limited to a zone just above 396 m below sea level (mbsl). Flares from this depth gained significant attention in the scientific community in recent years because they may be caused by bottom water-warming induced hydrate dissolution in the course of global warming and/or by recurring seasonal hydrate formation and decay. We found that gas emissions occurred widespread between about 80 and 415 mbsl which indicates that hydrate dissolution might only be one of several triggers for active hydrocarbon seepage in that area. Gas emissions were remarkably intensive at the main ridge of the forlandet moraine complex in 80 to 90 m water depths, and may be related to thawing permafrost.

Focused seafloor investigations were performed with the remotely operated vehicle (ROV) 'Cherokee'. Geochemical analyses of gas bubbles sampled at about 240 mbsl as well as at the 396-m gas emission sites revealed that the vent gas is primarily composed of methane (>99.70%) of microbial origin (average $\delta^{13}C = -55.7$ ‰ V-PDB).

Estimates of the regional gas bubble flux from the seafloor to the water column in the area of possible hydrate decomposition were achieved by combining flare mapping using multibeam and single beam echosounder data, bubble stream mapping using a ROV-mounted horizontally-looking sonar, and quantification of individual bubble streams using ROV imagery and bubble counting. We estimated that about $53 * 10^6$ mol methane were annually emitted at the two areas and allow a large range of uncertainty due to our method (9 to $118 * 10^6$ mol yr^{-1}). These amounts, first, show that gas emissions at the continental margin west of Svalbard were in the same order of magnitude as bubble emissions at other geological settings, and second, may be used to calibrate models predicting hydrate dissolution at present and in the future, third, may serve as baseline (year 2012) estimate of the bubble flux that will potentially increase in future due to ever-increasing global-warming induced bottom water-warming and hydrate dissolution.

Keywords: vent gas, hydroacoustic flare mapping, hydrate dissociation, global warming

1 Introduction

The Arctic is warming faster than any other region on earth, at the same time, gas hydrates in Arctic continental margins store significant amounts of methane (Archer and Buffett, 2005). As hydrates are stable at low temperature and high pressure conditions, gas hydrates in high-latitude regions that are characterized by relatively low bottom-water temperatures, can persist in relatively shallow water depths. Because those regions are highly sensitive to increases in bottom-water temperatures in the course of global warming shallow hydrates are highly susceptible to thermal dissociation, which might lead to methane release from the seafloor. Moreover, methane escaping the seafloor at shallow depths eventually reaches the atmosphere where it could contribute to the inventory of greenhouse gases. In that light, findings by Westbrook et al. (2009) were alarming: numerous gas emissions occurred at the continental margin west of Svalbard concentrated along a band at seafloor depths just above the 396-m isobath, which is the present top of the gas hydrate stability zone (GHSZ). During the last three decades the bottom water at that depth experienced a warming trend of 1°C (Westbrook et al., 2009). The authors assumed that the warming has induced a deepening of the upper boundary of the GHSZ from a depth of about 360 m 30 years ago to the present limit at 396 m, which could have caused hydrate dissociation in the sediments and, as a consequence, release of gas bubbles. The '396-m flares', as we call the site here, would be the first site where the hypothesis of global warming-induced hydrate dissolution may actually be confirmed.

Westbrook et al. (2009) offered an alternative hypothesis for the shelf-parallel occurrences of seafloor gas emissions. Free methane in deep continental slope sediments may migrate upward along the base of the GHSZ landward to the depths where it pinches out, which could also explain the clustering of gas emissions at 396 m depth. A prerequisite of this second hypothesis would be a capacious gas reservoir in deeper sediments supplying sufficient gas (primarily methane) to the gas emissions sites. Indeed, data available so far suggest that the continental margin west of Svalbard is prone to hydrocarbon seepage at the seafloor: the presence of gas hydrates (below ~600 m water depth) and free gas below the base of the GHSZ is indicated by the presence of a bottom simulating reflector (Vanneste et al., 2005; Westbrook et al., 2008; Chabert et al., 2011). In addition, hydrates were recovered from shallow sediments in ~900 m water depth (Fisher et al., 2011). Gas-related seismic facies occur at the upper slope and outer shelf (Sarkar et al., 2012; Rajan et al., 2012). Gas emissions occur at the 396-m flares on the upper slope but also at the outer shelf at water depths up to 150 m (Westbrook et al., 2009). Typical hydrocarbon seep-related bacterial mats were observed at the shelf (Knies et al., 2004). Elevated bottom-water methane concentrations and the stable carbon isotope composition of methane in the water column indicate seepage at the shelf (Damm et al., 2005; Gentz et al., 2014).

A third hypothesis of a seasonally varying thickness of the GHSZ was recently posed by Berndt et al. (2014). Uranium-Thorium-dating on massive methane-derived authigenic carbonates sampled at the seafloor at the 396-m flares ('MASOX site') revealed ages of up to three thousand years. These findings suggest a long history of methane venting, which argues against the hypothesis of recent global warming-induced hydrate decay. In addition, seasonal fluctuations of 1-2 °C in the bottom-water temperature measured with a seafloor-deployed mooring over a period of almost two years might cause periodic hydrate formation and dissolution (Berndt et al., 2014). However, a seasonally growing and declining thickness of the GHSZ should, consequently, result in seasonal fluctuations in gas bubble emissions, with more intensive emissions during the time of a retreating GHSZ from about June to December (warmer bottom water) and less intensive (or no) emissions from January to May (colder bottom water).

The amount of hydrate-bound methane that could potentially be released during dissociation was estimated in several modeling studies at the margin west of Svalbard but is still uncertain since reported numbers span about three orders of magnitude. The rates are given as annual amount of mol methane released from hydrate dissolution per meter of margin segment. The initially reported rate of global warming-induced release of hydrate-bound methane of 56.1 $*10^3$ mol yr^{-1} m^{-1} (Westbrook et al., 2009) was later scaled down to 8.8 $*10^3$ mol yr^{-1} m^{-1} (Reagan et al., 2011). For the future, a methane release rate from dissociating hydrates between 6.9 to 20.6 $*10^3$ mol yr^{-1} m^{-1} (10 years) and 13.2 to 72.3 $*10^3$ mol yr^{-1} m^{-1} (30 years) depending on different climate scenarios considered is expected (Marín-Moreno et al., 2013). Comparably high rates with up to 561 to

935 *10^3 mol CH_4 yr^{-1} m^{-1} kept or released in/from the seasonal gas hydrate mass were estimated by Berndt et al. (2014).

The main objective of this study is to quantify the amount of methane emitted as gas bubbles from the seafloor to the water column. We assume that most of the methane flux, is it derived from dissociating hydrate or directly from a free gas reservoir, is released as gas bubbles. Our study provides a useful mean of assessing the significance of the bubble flux, it can be used to calibrate models of hydrate dissolution, and, further, it can serve as base-line (year 2012) estimate of the methane flux that is likely to increase in future due to the ongoing warming trend. The quantification is based on the combination of ship-borne systematic hydroacoustic flare mapping and ROV-based estimation of the bubble flux of individual bubble streams. A further objective of our study is to map the distribution of gas emissions at the shelf and the upper continental slope west of Svalbard. Although we are not able to contribute to the ongoing discussion whether or not hydrate dissolution is the cause for the bubble emissions, flare distributions determined in the study area put the significance of the 396-m flares into perspective. Finally, samples of gas bubbles and geochemical analyses give insight into the genesis (thermogenic versus microbial) of emitted gas.

2 Study Area

The study area is located west of Svalbard (Fig. 1). The continental margin was shaped by the advances and retreats of the ice sheet covering Svalbard and the Barents Sea during the Pliocene-Pleistocene (Solheim et al., 1998; Vorren et al., 1998). Fast-flowing ice streams created the cross-shelf troughs seaward of the major fjord systems Kongsfjord and Isfjord. The inter-trough region west of Prins Karls Forland was covered by slow-flowing ice sheets with the shelf break marking approximately the seaward extent of the maximal ice coverage (Landvik et al., 1998). The shelf was flooded as glacial ice retreated about 13000 years ago (Landvik et al., 2005). Large areas of the shelf were mapped by the Norwegian Hydrographic Survey (Landvik et al., 2005) and the University of Tromsø (Ottesen et al., 2007). The existing multibeam data cover the shelf area east and north of the area shown in Figure 2 with some overlap in the central part. The forlandet morain complex is a pronounced ridge system at the middle slope with a crest in about 90 m water depth (Landvik et al., 2005). During a cruise in 2011 with the R/V James Clarke Ross gas emissions were found at the forlandet morain complex (Wright, 2012), an area that for simplicity we call Area 1 in the following. Additional evidence for hydrocarbon seepage at the shelf was presented by Knies et al. (2004) who discovered seep-typical sulfur-oxidizing bacterial mats using ROV.

The gas emissions discovered by Westbrook et al. (2009) are located at the outer shelf (Area 2 in this study) and upper continental slope (Area 3). The misalignment between gas vents at ~240 m water depth (Area 2) and at 396 m (Area 3) is caused by the combined action of a slump (Fig. 2) acting as seal for upward migrating fluids and glacigenic debris flows, which channel fluids along their base landward, as geophysical studies revealed (Rajan et al., 2012; Sarkar et al., 2012). Further landward of the prograding glacigenic sequences, pockmarks exist at the seafloor (Fig. 2) and a seismic image shows that one pockmark was underlain by an acoustic pipe structure but as no gas emissions were observed so far, they are probably relict structures of fluid emission (Rajan et al., 2012).

Two high-resolution seismic studies were carried out in the area of potential global-warming induced hydrate dissociation (Area 2 and 3) that led to different conclusions. The study by Rajan et al. (2012) focused on the region including Area 2 and the northernmost part of Area 3 (Fig. 2) that are affected by glacigenic debris flows. The authors imaged a gas cloud in the sediment below the landward limit of the GHSZ that they interpret as possible migration pathway of deep (thermogenic) gas. They conclude that the gas may be temporarily sequestered as gas hydrates but seismic evidence for this is lacking and, thus, any involvement of global-warming induced hydrate dissociation is speculative. However, based on a seismic data set covering the entire Area 3, Sarkar et al. (2012) argue, that evidence for fault-controlled gas migration from deeply-buried sediments, which could explain the contour-following trend of the flares originating at 396 m water depth is missing. Instead bright spots at shallow sediment depths close to the landward limit of the GHSZ, would be in accordance with global-warming induced hydrate dissolution.

While glacigenic sedimentation was predominant at the shelf and upper slope, the distal slope was influenced by hemipelagic sedimentation and bottom water currents, leading to the development of contourite drifts (Eiken and Hinz, 1993). Vestnesa Ridge is a contourite with evidence for a very active hydrocarbon venting system (Hustoft et al., 2009). Southeast of Vestnesa Ridge in Area 4 pockmark-like seafloor depressions exist between 800 and 1200 m water depth (Fig. 1). The presence of gas hydrates in the sediments was inferred from a well pronounced bottom simulating reflector (Sarkar et al., 2012) and proven by gravity coring (Fisher et al., 2011).

3 Material and Methods

The study is based on R/V Heincke cruise No. 387 (20 Aug to 9 Sept 2012) conducting research in the area west of Svalbard (Sahling et al., 2012). The multibeam echosounder Kongsberg Maritime EM 710 was employed for seafloor charting and water-column flare mapping. The system operates at frequencies between 70 and 100 kHz. It has 200 beams each with an opening angle of 1° across track and 2° along track. The footprint of the echosounder across track is therefore about 1.7% of the water depth. Two data sets for seafloor mapping (*.all files) and water column mapping (*.wcd files) were recorded (available online: http://doi.pangaea.de/10.1594/PANGAEA.816220). Seafloor data was processed with MB Systems (Caress and Chayes, 2001) and water column data with the program package by the company Quality Positioning Services BV (QPS) including FM Midwater and Fledermaus. Four sound velocity profiles were obtained during the cruise using a MIDAS sound velocity probe (company Valeport).

Scientific single beam echosounder EK 60 operates with up to four frequencies but for the purpose of this study, only the 38 kHz frequency was analyzed for mapping and flare classification purposes. Data were recorded with the ER 60 software, stored as *.raw files (available online: http://doi.pangaea.de/10.1594/PANGAEA.816056), and processed using the readEKRaw MATLAB toolkit (by Rick Towler, NOAA Alaska Fisheries Science Center; available online: http://hydroacoustics.net/viewtopic.php?f=36&t=131).

The toolkit was used to convert the data into Sv, which is the volume backscattering per unit volume expressed in dB re 1 m^{-1}. Sv is often used when individual targets are very small in the sampled volume as several echoes are combined to give a certain signal level. A toolkit for mapping flares was designed. This consists of an interface where the user is reading echosounder traces and is asked to pick manually the flares that appear. For each selected flare, an Id (with the format DayMonthNumbering) is given and its characteristics are stored (Supplementary material S1): the date and time at which it was observed, its longitude and latitude, its strength as the weighted sum of all Sv levels within its trace area, and finally its height. The weighted sum of all Sv levels was made on a linear scale with the purpose of classifying flares into strong and weak. Locations of flares were plotted with GMT using color coding for classifying strong and weak flares (threshold arbitrarily set at 4 dB re 1 m^{-1}; Fig. 2).

The remotely operated vehicle (ROV) MARUM-Cherokee is a mid-size inspection class vehicle manufactured by Sub-Atlantic, Aberdeen. Underwater positioning was obtained using the ultra-short baseline system GAPS by Ixsea. Scientific payload of the ROV was a modified, small-sized version of the pressure-tight Gas Bubble Sampler (GBS; Pape et al., 2010), custom made bubble catchers, and horizontally scanning sonars (Imagenex 881A or Tritech) mounted on top of the vehicle to allow 360° sonar view. Still images were acquired with a 5 megapixel Kongsberg OE-14 camera. Videos were recorded with a Tritech Typhoon PAL camera and stored electronically in AVI format.

The volume flux of bubbles was estimated using a bubble catcher and visually using the video. Scaling of the images was obtained by placing objects of known dimensions (such as the ROV-manipulator) into the plane where the bubbles occur. Due to the low shutter speed, bubbles appear blurred as long ellipsoids in the video frames and, therefore, only one bubble diameter could be measured. From each measure, volumes were calculated assuming spherical bubbles and fluxes were inferred by multiplying the average bubble volume with the emission frequency. The volume flux was then converted to mass flux assuming that the gas consists of pure methane and considering the compressibility of methane (compressibility = 0.91 at 380 m water depth, 39 bar, 4 °C; compressibility = 0.93 at 240 m water depth, 25 bar, 4 °C). A SBE911plus Sea-Bird Electronic CTD was used to acquire hydrographic parameters. Gas collected with the GBS was analyzed with a two-channel 6890 N (Agilent Technologies) gas chromatograph described in detail in Pape et al. (2010). Hydrate phase boundaries were calculated using the HWHYD U.K. software (Masoudi and Tohidi, 2005).

4 Results

4.1 Flare mapping

A total of 1920 nautical miles of hydroacoustic profiles were acquired during the He-387 cruise (Fig. 1). For simplicity, we subdivided the region in five areas. Flares in the water column were found at the continental shelf (Area 1), close to the shelf break (Area 2), and at the upper continental slope (Area 3), but not above the pockmarks (Area 4), and along the 396-m depth contour further north (Area 5).

Numerous flares occurred at the shelf and upper slope west of Prins Karls Forland (Fig. 2). Gas emissions concentrate in Areas 1, 2, and 3. Emission sites in Areas 2 and 3 correspond to those discovered by Westbrook et al. (2009) at water depth around 240 m and 396 m, respectively. We focused on quantifying the amount of gas emitted in these areas (Sec. 4.3 and 4.4). In addition, we found numerous gas emissions on the shelf at water depths of about 80 to 90 m and particularly from a ~50 m high ridge (Area 1) that is part of the forlandet morain complex (Landvik et al., 2005). Gas bubble emissions occurred in clusters on the ridge and even more flares were recognized close to the rim of the plateau on top of the ridge.

In addition to gas emissions in the three main areas (Areas 1-3), flares were found widespread at the shelf. Those flares occurred more dispersed compared to the aggregations at the forlandet morain complex and their relative intensity was generally weak compared to those recorded in Areas 1, 2, and 3. Flares preferentially occurred on topographic highs such as shelf break-parallel ridges that we interpret as recessional moraines. It should be noted, however, that the distribution of the flares as shown in Figure 2 is biased by the survey line spacing. Dense line spacing increases the chance to hit a bubble emission, therefore, the track line of the ship is plotted in Figure 2 as well. Another topographic feature on the shelf with a considerable number of gas emissions is the transverse ridge at the northern border of the Isfjord cross-shelf trough. More survey lines would be needed to unravel if this feature might also be a significant source region for gas emissions.

We found no evidence for gas bubble emission in Area 4 (Fig. 1) connected to pockmarks, which are rounded to elongated depressions at the seafloor at depths between about 800 and 1200 m. Sixteen pockmarks were crossed during our hydrocaoustic surveys but flares have not been detected in the EK 60 records. While pockmarks are generally considered as traces of cold fluid seepage, we conclude that gas bubble emission was not active at the time of investigation.

The ~396 m depth contour is the relevant depth, where flares would be expected to occur, if one or both of the hypotheses of global-warming induced hydrate dissolution or a seasonal GHSZ are correct. Therefore, we expanded our survey along this depth for about 80 km to the north (Area 5). However, during this survey we found no evidence for bubble emissions neither in the EM 710 nor in the EK 60 records suggesting that the 396-m flares were restricted to Area 3 west of Prins Karls Forland.

4.2 ROV-based observations and vent gas composition

In total we conducted nine remotely operated vehicle (ROV) dives in Areas 1, 2, and 3 (Table 1). The seafloor at Area 1 (80 to 90 m water depth), that is located at the main ridge of the forlandet moraine complex, was composed of cobble to boulder-sized rocks (Fig. 3A) that we interpret as glacial till. Fine grained sediment filled the space between rocks. Bivalve shells, living sea urchins and other hardground biota were observed. Bubble emission sites in Area 1 were patchily distributed. Bubbles rose through rocks or fine grained sediments, with, in the latter case, whitish microbial mats associated.

In Area 2 (240 to 245 m water depth) the proportion of soft sediment was higher compared to Area 1. However, similar to Area 1 cobble to bolder-sized rocks of glacigenic origin occurred. In addition, rocks resembling methane-related authigenic carbonates were found associated to bubble streams. Bubbles were released from cm-sized fractures. In places crusts were fractured exposing cavities below the crust (Fig. 3B). At some sites bubbles accumulated below crusts leading to a periodic release of bursts of bubbles alternating with times of quiescence. Microbial mats were observed on soft sediments and around bubble emissions on hard ground.

In Area 3 ('396-m flares'), ROV dives were carried out at three locations. In general, the proportion of soft sediments again was higher compared to that at the shallower sites. As found in Area 2, crusts resembling methane-related authigenic carbonates were present. Microbial mats occurred around bubble emission sites on rocks and on soft sediments. Pogonophoran tubeworms (Siboglinidae) covered by microbial mats were observed (Fig. 3F). Swarms of demersal fish were encountered.

Analysis of the composition of gas bubbles sampled with the GBS at six bubble streams in all three areas showed that the gas from Areas 2 and 3 is generally dominated by methane (99.70 to 99.99% ($\Sigma(C_1$-C_3, $CO_2)$); Table 2). Only the single gas sample from Area 1 (90 m) contained a noticeable fraction of CO_2 (~1%). The C_1/C_2 ratio of all samples ranged between 7800 and 15000.

4.3 Quantification of gas fluxes in Area 2 (240 - 245 m)

In order to conduct an order-of-magnitude estimate of the flux of gas emitted in Area 2, we followed a simple approach: at first, we quantitatively mapped flares using the water column data acquired with EM 710. During ROV-dives we found out that bubble streams occurred in cluster. While one bubble stream may be enough to cause a flare in several instances more than one stream was encountered in most cases. We therefore studied several clusters and estimated the number of bubble streams per cluster. Finally, we estimated the flux of methane emitted per bubble stream. We then estimated the flux of methane for the entire area by conducting minimum and maximum estimations that encompass a wide range of uncertainty.

In order to quantitatively map flares in Area 2, we used the water column data recorded by EM 710 as illustrated in Figure 4. The EM 710 survey was designed in such a manner that almost complete coverage of the area (gray-shading in Figure 5) was achieved while significant overlap could be avoided. In total, 512 flares originating from the seafloor in about 240 to 245 m water column were picked from the EM 710 water column data. Most flares concentrated along lineaments trending parallel to the shelf break. The shelf in this area is flat without discernable morphology based on the swath bathymetry.

Flare intensities varied, but due to noisy EM 710 data classification of flare intensities (weak vs. strong) could not be achieved, this was left to the EK60 data. Two ROV dives were conducted in Area 2 (Fig. 6) at sites where weak and strong flares occurred close to each other (Table 1). For practical reasons, we termed a site where we found one or more gas emissions within a small area a 'cluster'. The appearance of cluster C6 in the sonar record is shown in Figure 7. Within a distance of less than ~ 3 m, we observed 5 bubble streams (S1-S5). We assumed that all these bubble streams contributed to a flare imaged with EM 710 because the distance between the streams (max. 3 m) was smaller than the footprint size of the EM 710 (about 5 m; 1.7% of water depth). In total, we found six clusters composed of 1 to 15 bubble streams (average ~6) in Area 2 (Table 3).

At 15 individual bubble emission sites (at 5 different clusters) we either calculated the gas volume flux by interpreting ROV-based videos (visual quantification) or measured it by placing an inverted funnel (bubble catcher) over the streams (Figs. 3 C and D). Application of both methods at two emission sites showed that the differences were less than 25% (Table 3). On average, 15.2 ml min^{-1} of gas (std. dev. = 7.5 ml min^{-1}, n = 15) were emitted from an emission site. Assuming that the bubbles consisted of pure methane these rates correspond to methane flux rates of 17 ± 8 mmol min^{-1}.

Based on the flux rates mentioned above, we estimated the flux of methane as gas bubbles from the seafloor for the entire Area 2. Multiplying the number of 512 known flares existing in Area 2 with average numbers of 6 individual bubble streams per cluster (Table 3), and average methane flux rates at each bubble stream (17 mmol min^{-1}), and assuming that the gas is pure methane, 52 mol CH_4 min^{-1} are emitted in Area 2.

We further estimated minimum and maximum flux rates by considering the uncertainties inherent to the approach. An uncertainty of more than one order of magnitude is introduced by the number of bubble streams feeding a flare as it varied between 1 and 15 (Table 3). The variability of the flux of a bubble stream

(17 ± 8 mmol min^{-1}) is comparably small (less than factor 2). Furthermore, we regard other potential sources of errors not detailed here as comparably negligible. Calculated minimum and maximum fluxes, which solely considered that between 1 and 15 bubble streams were found to feed a flare, resulted in flux rates ranging between 9 and 130 mol min^{-1}, respectively. Assuming a constant flux over time, the above mentioned values translate to 27 x 10^6 (min: 5 x 10^6, max: 68 x 10^6) mol CH_4 yr^{-1}.

4.4 Quantification of gas fluxes in Area 3 ('396-m flares')

We quantitatively looked for gas emissions with the EM 710 in Area 3 at the upper continental slope (Fig. 8). The distribution of flares was similar to early observations of Westbrook et al. (2009) and confirmed that the majority of flares are located at an interval between 360 and 415 m water depths.

Preliminary results during our cruise revealed that flares were difficult to pick in the EM 710 data as they were not stable over time and due to the fact that the location of flares at the seafloor varied. Therefore, we used a statistical approach as we were mainly interested in the question of how many flares occur in Area 3 at any given time. For this approach we used four equally spaced hydroacoustic profiles running across the area where most flares group together. By plotting all flare positions picked from the EM 710 record (Fig. 8), we identified that more than 90% of the flares detected in Area 3 occurred in a restricted NW-SE trending 'seep area' (Fig. 8). We used the data obtained during the four transects crossing this 'seep area' to determine the number of flares during each crossing (Fig. 9). Because each crossing covered only part of the 'seep area' we calculated the total number of flares by assuming that the flares were regularly distributed. Subsequently, we counted the number of flares within the observed area, which is the seep area within the footprint of the EM 710 (e.g. the red rectangle in Fig. 9A) and extrapolate that number to the entire seep area (Table 4). The resulting average number of flares within the 'seep area' was 452. The observed range (min. = 384, Fig. 9D; max. = 524, Fig. 9B) gave an indication of the uncertainty inherent to the methodology used and the variability of gas emissions.

The temporal variability of bubble emissions was confirmed during ROV dives. We found that individual bubble streams were transient with bubbles being emitted for seconds or tens of seconds followed by minutes of inactivity. In addition, the sites of emission changed spatially within a few decimeters. We estimated the number of bubble streams occurring in cluster by observing the area using the horizontally looking sonar for several minutes per site and counted the number of streams that became visible during the observation time. The numbers given in Table 5 reflect maximum values: at a given moment bubbles were emitted only from some sites, i.e. only a fraction of the total number of emission sites was active. The quantified volume flux at several bubble streams resulted in 20.9 ml min^{-1} on average (Table 5). The high variability is reflected in a large standard deviation of 15.9 ml min^{-1} (n = 8). The values correspond to a mass flux of 18.3 ± 9.1 mmol min^{-1} assuming pure methane.

The total seafloor flux of methane in Area 3 was calculated based on the following numbers: Considering average numbers of flares (n = 452) and of bubble streams per cluster (n = 6) and an average CH_4 mass flux (18.3 mmol min^{-1}), about 50 moles of methane per minute are emitted in Area 3. Because the uncertainty inherent to this approach is expectedly large, we conducted estimations of the minimum and maximum flux. If we consider that only 384 flares occur in Area 3 (Table 4) and assume that each flare may be sourced by a single bubble stream with an average CH_4 mass flux only, this results in a seafloor methane flux of 7 mol min^{-1} in Area 3. Calculation of the maximal flux considering the maximum numbers of flares (n = 523) and of bubble streams found in a cluster (n = 10) and average mass fluxes, resulted in 96 mol CH_4 min^{-1} in Area 3. These values correspond to fluxes of 26 x 10^6 (min. 4 x 10^6, max. 50 x 10^6) mol CH_4 yr^{-1}.

5 Discussion

5.1 Sources of methane

Traditionally, light hydrocarbons of microbial and thermogenic origin are distinguished by the relation of their molecular composition and the methane stable carbon isotope ratio (e.g. Whiticar, 1990). The molecular composition of gas in bubbles collected with the GBS several centimeters above the seafloor in Areas 2 (240 to 245 mbsl) and Area 3 ('396-m flares') indicate a predominantly microbial origin of the vent gas (C_1/C_2 ca. 9,700 to 15,200; Fig. 10). However, less negative $\delta^{13}C-CH_4$ ratios (–53.8 to –57.4‰ V-PDB) than expected from the molecular composition for typical microbial methane point to some admixture of methane enriched in ^{13}C. A possible explanation for this observation might be that part of the methane has undergone oxidation within the sediments, which would result in ^{13}C-enrichment of the residual methane.

Our finding of gas with an average $\delta^{13}C$ ratio of –55.7‰ in Areas 2 and 3 complements well results from water column studies in Area 2 carried out by Gentz et al. (2014). Using correlations between concentration and stable carbon isotopic compositions of methane in the water column the authors inferred the C-isotope signature of methane emitted from the seafloor (about –60‰). A similar $\delta^{13}C$ ratio (–54.6 ± 1.7‰) was reported by Fisher et al. (2011) for methane in hydrates recovered from an area termed 'Plume field' (890 m water depth), which is identical to our Area 4. In summary, the source of methane at the upper continental slope and outer shelf (Areas 2, 3, and 4) appear to be similar based on its geochemical signature and largely microbial in origin.

Gas emitted as bubbles at the shelf in Area 1 (~90 m water depth) differs from that sampled in Areas 2 and 3 in its molecular composition (C_1/C_2 ca. 7,850) and $\delta^{13}C-CH_4$ ratio (–43.5‰ V-PDB) (Fig. 10). This difference is significant, but only a single gas sample could be obtained from Area 1 during our research cruise. Nevertheless, this finding generally agrees with the water column study by Damm et al. (2005) carried out on a much larger scale along the entire SW continental margin of Svalbard. The authors postulated widespread methane seepage along the shelf with respect to methane enrichments at several stations. In addition, the authors observed a topography-dependent methane isotope signature with –30‰ at the tops and –49‰ in troughs. Damm et al. (2005) conclude that the geochemical signature of methane is influenced due to its slow seepage through the sediments leading to 'inter-granular seepages or micro-seepages'. Our results clearly show that methane emission at the shelf is not limited to micro-seepage, but also occurs as vigorous bubble emission as observed at the main ridge of the forlandet moraine complex.

Unfortunately, our sparse results on the gas composition and methane isotope signature at the forlandet moraine complex do not allow any final assessment of the source of methane (Fig. 10) because migration, oxidation, and in situ generation of gas might have overprinted the original signature. Additional gas samples (e.g. from the deeper subsurface) are needed to ultimately clarify this aspect.

5.2 Distribution of gas emissions at the seafloor

The results of our extensive hydroacoustic survey (single beam and swath mapping) provide valuable insight into the system of gas emission at the continental margin west of Svalbard. We have covered large areas searching for flares with hydroacoustic techniques (Fig. 1), but evidence for gas emissions was restricted to the region west of Prins Karls Forland. This region is apparently prone to fluid flow as suggested by gas emissions occurring all over the shelf and upper slope. Gas emissions exclusively occur in this inter-fan region bordered by the Kongsfjord cross-shelf trough to the north and the Isfjord cross-shelf trough to the south.

The swath bathymetry acquired during our cruise significantly extends published maps (Landvik et al., 2005; Ottesen et al., 2007) and shows a series of along-shelf, parallel ridges between the shelf break and the forlandet moraine complex (Fig. 2). We interpret these ridges as surface expressions of prograding foresets, which are sediments deposited at the seaward termination of ice sheets during phases of progression and regression. Because seismic data acquired in the region comprising Areas 2 and 3 show prograding glacigenic sequences at the outer shelf (Rajan et al., 2012; Sarkar et al., 2012), it can be expected that these also occur further to the south. Gas emissions occur all over the shelf with a peculiar clustering at the forlandet moraine complex. In contrast, the distribution of gas emissions at the shelf distant to the forlandet moraine complex does not follow any discernable pattern; however, there might be a weak tendency that flares preferentially occur at topographic highs but not in depressions.

Numerous flares concentrated at the forlandet moraine complex at water depth of about 80 to 90 m (Fig. 2). The detailed hydroacoustic surveys conducted during our cruise revealed that almost all flares originated from the top of the moraine, which suggests that the methane source might be located within the morphological ridge itself. However, as we lack data on the sub-seafloor structure, this remains speculative. Potential capacious methane reservoirs at Arctic continental shelves are methane-loaded sediments below permafrost (e.g. Rachold et al., 2007). Transgression of the ocean following the last glacial stage has led to submergence and subsequent dissolution of permafrost in the sediments induced by bottom-water temperatures >0°C. In case the permafrost seal is broken, methane can escape the reservoir and may be emitted as bubbles from the seafloor, a process recently observed on large scales at the East Siberian Shelf (Shakova et al., 2010). Still ongoing permafrost melting may, thus, be an explanation for the concentrated gas emissions observed at the forlandet moraine complex. In case this holds true, a microbial origin of the expelled gas would be expected. Unfortunately, the geochemical properties of the gas sample collected in Area 1 do not allow for unambiguous source assignments. Additional sub-surface gas samples are needed to unravel the gas source at the forlandet moraine complex.

Flares in Areas 2 and 3 are potentially sourced by dissociating gas hydrates (Westbrook et al., 2009; Berndt et al., 2014). Bubbles in Area 2 are emitted at shallow depth of about 240 to 245 m above the GHSZ. Seismic studies, however, have shown that the flares may also be sourced by dissociating hydrates (Rajan et al., 2012; Sarkar et al., 2012). A slump at the upper slope and prograding forsets led to the landward deviation of upward migrating fluids, such that the gas is emitted along lineaments at the outer shelf (Fig. 5).

Flares in Area 3 are linearly orientated along a band at the upper continental slope at water depth above ~396 m (Fig. 8). Using the swath echosounder, we systematically mapped the upper slope in order to quantitatively record the occurrence of flares in Area 3. In accordance with earlier observations we found that the majority of gas emissions occurred along a narrow band (gray shaded 'seep area' in Fig. 8) with some additional flares located above and below that area, a pattern that was attributed to small-scale lithological heterogeneity before (Sarkar et al., 2012).

While our results do not allow to conclude whether methane emissions in Area 3 are fed by dissociating gas hydrates, we are able to refine the depth-dependent flare distribution already proposed before Westbrook et al. (2009) with our data. The abundance of flares versus depth in Area 3 is shown in Figure 11. Because the depth-related abundance of flares resembles a Gaussian distribution a generic link between depth and gas emission is intuitive.

Because most flares occurred between about 360 and 415 m water depth it is tempting to calculate the sediment temperature increase which would be required to induce hydrate dissociation. For this, we calculated the gas hydrate phase boundary using the composition of gas sample GeoB 16833-2 collected with the GBS (Fig. 11). The resulting increase in sediment temperature of 1.2 °C is in agreement with both hypothesis proposed to explain the narrow zone of flare origins at the seafloor: a 1°C temperature increase during the last 30 years (Westbrook et al., 2009) and a seasonal fluctuation of 1–2 °C as measured with the MASOX lander (Berndt et al., 2014).

Based on the seafloor flare distribution determined in this study, we conclude that if gas hydrate dissolution is a cause for seafloor gas emissions, this process was spatially limited to one segment at the continental margin (west of Prins Karls Forland) during the time of our investigation. Furthermore, the presence of numerous additional flares at the shelf suggests that this particular region west of Prins Kalrs Forland is prone to hydrocarbon seepage and that gas seafloor emission unaffected by gas hydrate dissociation is common in the region.

5.3 Quantification of gas bubble emissions

Combining hydroacoustic data with ROV-based observations, we quantified the flux of methane as gas bubbles from the seafloor to the water column. This approach is advantageous because it is relatively simple and straight forward providing order-of-magnitude estimations for gas bubble fluxes. Similar methodologies were recently applied in other settings characterized by gas bubble emissions (Römer et al., 2012a; Römer et al., 2012b; Römer et al., 2014; Sahling et al., 2009).

Here, we discuss two major sources of uncertainty in our flux calculations that we regard as most important. Our estimation is a snapshot in time, taken at a few days in Aug/Sept 2012. This is especially important in light of the recently posed hypothesis (Berndt et al., 2014) that a temperature-induced annual build-up and break-down of hydrates would lead to an annual cycle in the gas emissions. Our results show that the gas emissions were persistent for hours (ROV-observations) or even days (repeated hydroacoustic observations, Fig. 9; Tab. 4). In addition, gas emissions were encountered each year since their discovery in 2008 (Westbrook et al., 2009): 2009 (Fisher et al., 2011; Rajan et al., 2012), 2010 (Gentz et al., 2014), 2011 (Wright, 2012), 2012 (Berndt et al., 2014; this study). All investigations of gas emissions in that region so far were carried out in the summer period, and, therefore, it is uncertain whether the gas emissions undergo annual periodicity. In order to test the hypothesis by Berndt et al. (2014), a research campaign in spring, when bottom water temperatures are minimal and the thickness of the GHSZ should peak (and thus bubble emission may be minimal), would be useful. In this study, we state gas fluxes per year for comparative purposes (see below) although the temporal variability of gas emissions is unknown.

Our quantification approach revealed a source of uncertainty that waits for a technical solution, i.e. an answer to the question how many individual streams of bubble contribute to one flare as imaged by ship-mounted multibeam echosounder. By use of the ROV-mounted horizontally-looking sonar we found that a single bubble stream is enough to cause a flare but that sometimes up to 15 bubble streams contribute to one flare (Table 3). While the bubble flux of a single bubble stream can appropriately be determined by using a ROV (visually or by capturing the bubbles), and the numbers of flares can be systematically mapped using multibeam, the uncertainty in the bubble stream-to-flare ratio introduces a factor of >10. In this study, we employed the ROV-mounted sonar for this purpose but encountered several shortages, i.e. the difficulty to keep the ROV stationary at strong bottom-water currents and the need of very long scanning times consuming a lot of highly valuable ROV operation time. A towed sonar system or a sonar on a bottom-mounted lander system would be desirable technical innovations.

The bubble flux of methane in Areas 2 (5 to 68 * 10^6 mol yr^{-1}) and 3 (4 to 50 * 10^6 mol yr^{-1}) estimated in this study, is similar to the range of fluxes (0.23 to 87 * 10^6 mol yr^{-1}) in other bubble emission settings (Table 6). Because bubble fluxes in all these settings are in the same order of magnitude gives confidence that our approach used for estimating the flux in this study is reliable.

Our estimation of the bubble flux contributes to the ongoing discussion about the amount of gas hydrate in the upper continental slope west of Svalbard that is susceptible for temperature changes. We base the following discussion on the assumption that most of the methane is released as gas bubbles from the seafloor, when hydrates within the seafloor are dissociating. We neglect the amount of methane that is consumed by oxidation within the seafloor or that is emitted dissolved in the aqueous phase, as we have no control on these processes. In order to compare flux rates determined in this study with those given in the literature for hydrate dissociation, we converted published rates into the annual methane flux per meter margin segment (mol m^{-1} yr^{-1}). Our systematic flare mapping revealed that the gas emission-influenced margin segment has a length of ~14 km (Areas 2 and 3, Fig. 5 and 8), which is short compared to those (30 and 25 km, respectively) investigated in other related studies (Westbrook et al., 2009; Marín-Moreno et al., 2013).

Overall, the bubble flux estimated in this study is lower than the amount of methane released from dissociating hydrates reported earlier (Table 7). However, the published rates span three orders of magnitude with minimum rates being consistent with our estimates. Westbrook et al. (2009) initially estimated methane release from dissociating hydrates at about 56 * 10^3 mol m^{-1} yr^{-1}. Based on 2D modeling (Reagan et al., 2011) scaled this value down to 8.8 * 10^3 mol m^{-1} yr^{-1}, which is about the same order of magnitude as our bubble-flux estimate (0.6 to 8.4 * 10^3 mol m^{-1} yr^{-1}). These fluxes are based on an increase in bottom-water temperature of about 1°C during the past three decades considering progressive hydrate dissolution at present. If the gas emission in Areas 2 and 3 are sourced by temperature-induced multi-year hydrate dissolution, the model by Reagan et al. (2011) appear to be most applicable.

The impact of future bottom-water warming on hydrates in sediments of the upper continental slope west off Svalbard was modeled by Marín-Moreno et al. (2013)

using climate models and scenarios representing low and high greenhouse emissions (i.e. representative concentration pathways 2.6 and 8.5, respectively). During the upcoming 100 years, the hydrate dissolution rate is forecasted at 6.9 to 20.6 * 10^3 mol m^{-1} yr^{-1} with acceleration to 13.2 to 72.3 * 10^3 mol m^{-1} yr^{-1} within the next 300 years. These rates are, again, higher compared to those determined for present bubble emissions in this study. The predictions by Marín-Moreno et al. (2013) call for monitoring of the hydrate deposits west of Svalbard in the future.

According to Berndt et al. (2014) release of methane from the dynamic hydrate reservoir amounts to 561 to 935 * 10^3 mol m^{-1} yr^{-1}, which is two orders of magnitude higher than the bubble flux that we estimate. The discrepancy between these values warrants further investigation. A first approach could be, to test whether bubble emission intensities actually vary during the year.

Because methane is a potent greenhouse gas, the fate of methane emitted from the seafloor is of relevance. Gentz et al. (2014) showed for the well-stratified water column in Area 2 during the summer that the majority of methane is diffusing from bubbles into the water column below the pycnocline and leads to relative enrichments in the concentrations of dissolved methane in the lower water body. However, as the lower water body is isolated from the upper water layer by the density difference (the pycnocline), methane dissolved in lowermost water masses does not reach the atmosphere. Therefore, most of the methane emitted from the seafloor is either oxidized, or transported in the water mass and further diluted, or reaches the sea surface, where it could escape into the atmosphere. Complete methane removal by oxidation occurs within about 50 to 100 days (Gentz et al., 2014). Therefore, the fate of methane depends on the timeframe and fate of the water mass. The situation is different in autumn, when storms and low temperatures break down the water column stratification and induce vertical mixing. Although not studied so far, it might be expected that bubble-forming methane gets dissolved in the water and transported through the water-air interface into the atmosphere, contributing to the atmospheric methane inventory.

6 Conclusion

At the upper slope (Area 3) and outer continental shelf (Area 2) methane of microbial origin is emitted at the seafloor. Based on our data, we cannot contribute to the question if gas hydrate dissolution is the cause for the observed bubble emissions and, further, if a multi-year warming trend (1°C in 30 years) or a seasonal temperature cycle is the driver of the hydrate dissolution. But our data show that if hydrate dissolution in Areas 2 and 3 occurs, it is spatially limited to a margin segment of about 14 km and does not occur along the ~80 km 396-m isobath to the north. Our quantification of gas emissions in Areas 2 and 3 reveals methane fluxes in the same order of magnitude as found at bubble vents in other geological settings. If hydrate dissociation is involved, our flux estimate may help to refine models on this temperature-susceptible reservoir and serves as baseline, in the case that warming leads to intensified gas emissions in future.

The gas emissions in Areas 2 and 3 are only one aspect of fluid flow offshore Svalbard as bubble vents were found all over the shelf and especially prominent at the forlandet moraine complex (Area 1) reflecting that the area west of Prins Karls Forland is prone the gas venting. We speculate that decaying permafrost may allow methane to escape from a deeper reservoir at the forlandet moraine complex at water depth around 90 m.

Acknowledgement

We thank the captain and crew of R/V Heincke cruise 387. This work was funded through the DFG-Research Center/Excellence Cluster "The Ocean in the Earth System" MARUM – Center for Marine Environmental Sciences. M. T. was supported by SENSEnet, a Marie Curie Initial Training Network funded by the European Commission 7th Framework Program, Contract No. PITN-GA-2009-237868.

References

Archer, D., and Buffett, B.: Time-dependent response of the global ocean clathrate reservoir to climate and anthropogenic forcing, Geochem. Geophys. Geosy., 6, Q03002, doi:10.1029/2004GC000854, 2005.

Berndt, C., Feseker, T., Treude, T., Krastel, S., Liebetrau, V., Niemann, H., Bertics, V. J., Dumke, I., Dünnbier, K., Ferré, B., Graves, C., Gross, F., Hissmann, K., Hühnerbach, V., Krause, S., Lieser, K., Schauer, J., and Steinle, L.: Temporal constraints on hydrate-controlled methane seepage off Svalbard, Science, 343, 284-287, doi:10.1126/science.1246298, 2014.

Chabert, A., Minshull, T. A., Westbrook, G. K., Berndt, C., Thatcher, K. E., and Sarkar, S.: Characterization of a stratigraphically constrained gas hydrate system along the western continental margin of Svalbard from ocean bottom seismometer data, J. Geophys. Res., 116, B12102, doi:10.1029/2011jb008211, 2011.

Damm, E., Mackensen, A., Budéus, G., Faber, E., and Hanfland, C.: Pathways of methane in seawater: Plume spreading in an Arctic shelf environment (SW-Spitsbergen), Cont. Shelf Res., 25, 1453-1472, 2005.

Eiken, O., and Hinz, K.: Contourites in the Fram Strait, Sediment. Geol., 82, 15-32, doi:10.1016/0037-0738(93)90110-Q, 1993.

Fisher, R. E., Sriskantharajah, S., Lowry, D., Lanoisellé, M., Fowler, C. M. R., James, R. H., Hermansen, O., Lund Myhre, C., Stohl, A., Greinert, J., Nisbet-Jones, P. B. R., Mienert, J., and Nisbet, E. G.: Arctic methane sources: Isotopic evidence for atmospheric inputs, Geophys. Res. Lett., 38, L21803, doi:10.1029/2011gl049319, 2011.

Gentz, T., Damm, E., Schneider von Deimling, J., Mau, S., McGinnis, D. F., and Schlüter, M.: A water column study of methane around gas flares located at the West Spitsbergen continental margin, Cont. Shelf Res., 72, 107-118, doi:10.1016/j.csr.2013.07.013, 2014.

Hustoft, S., Bünz, S., Mienert, J., and Chand, S.: Gas hydrate reservoir and active methane-venting province in sediments on <20 Ma young oceanic crust in the Fram Strait, offshore NW-Svalbard, Earth Planet. Sc. Lett., 284, 12-24, doi:10.1016/j.epsl.2009.03.038, 2009.

Jakobsson, M., Macnab, R., Mayer, L., Anderson, R., Edwards, M., Hatzky, J., Schenke, H.-W., and Johnson, P.: An improved bathymetric portrayal of the Arctic Ocean: Implications for ocean modeling and geological, geophysical and oceanographic analyses, Geophys. Res. Lett., 35, doi:10.1029/2008GL033520, 2008.

Knies, J., Damm, E., Gutt, J., Mann, U., and Pimnturier, L.: Near-surface hydrocarbon anomalies in shelf sediments off Spitsbergen: Evidence for past seepages, Geoch., Geophys., Geosy., 5, doi:10.1029/2003GC000687, 2004.

Landvik, J. Y., Bondevik, S., Elverhoi, A., Fjeldskaar, W., Mangerud, J., Salvigsen, O., Siegert, M. J., Svendsen, J.-I., and Vorren, T. O.: The last glacial maximum of Svalbard and the Barents Sea area: Ice sheet extent and configuration, Quaternary Sci. Rev., 17, 43-75, 1998.

Landvik, J. Y., IngÓLfsson, Ó., Mienert, J., Lehman, S. J., Solheim, A., ElverhØI, A., and Ottesen, D. A. G.: Rethinking Late Weichselian ice-sheet dynamics in coastal NW Svalbard, Boreas, 34, 7-24, doi:10.1111/j.1502-3885.2005.tb01001.x, 2005.

Marín-Moreno, H., Minshull, T. A., Westbrook, G. K., Sinha, B., and Sarkar, S.: The response of methane hydrate beneath the seabed offshore Svalbard to ocean warming during the next three centuries, Geophys. Res. Lett., 40, 5159-5163, doi:10.1002/grl.50985, 2013.

Masoudi, R., and Tohidi, B.: Estimating the hydrate zone in the presence of salts and/or organic inhibitors using water partial pressure, J. Petrol. Sci. Eng., 46, 23-36, doi:10.1016/j.petrol.2004.10.002, 2005.

Ottesen, D. A. G., Dowdeswell, J. A., Landvik, J. Y., and Mienert, J.: Dynamics of the Late Weichselian ice sheet on Svalbard inferred from high-resolution sea-floor morphology, Boreas, 36, 286-306, doi:10.1111/j.1502-3885.2007.tb01251.x, 2007.

Pape, T., Bahr, A., Rethemeyer, J., Kessler, J. D., Sahling, H., Hinrichs, K.-U., Klapp, S. A., Reeburgh, W. S., and Bohrmann, G.: Molecular and isotopic partitioning of low-molecular-weight hydrocarbons during migration and gas hydrate precipitation in deposits of a high-flux seepage site, Chem. Geol., 269, 350-363, doi:10.1016/j.chemgeo.2009.10.009, 2010.

Rachold, V., Bolshiyanov, D. Y., Grigoriev, M. N., Hubberten, H.-W., Junker, R., Kunitsky, V. V., Merker, F., Overduin, P., and Schneider, W.: Nearshore arctic subsea permafrost in transition, Eos, 88, 149-150, 2007.

Rajan, A., Mienert, J., and Bünz, S.: Acoustic evidence for a gas migration and release system in Arctic glaciated continental margins offshore NW-Svalbard, Mar. Petrol. Geol., 32, 36-49, doi:10.1016/j.marpetgeo.2011.12.008, 2012.

Reagan, M. T., Moridis, G. J., Elliott, S. M., and Maltrud, M.: Contribution of oceanic gas hydrate dissociation to the formation of Arctic Ocean methane plumes, J. Geophys Res.-Oceans, 116, C09014, doi:10.1029/2011jc007189, 2011.

Römer, M., Sahling, H., Pape, T., Bahr, A., Feseker, T., Wintersteller, P., and Bohrmann, G.: Geological control and quantity of methane ebullition from a high-flux seep area in the Black Sea - the Kerch seep area, Marine Geology, 319-322, 57-74, 2012a.

Römer, M., Sahling, H., Pape, T., Bohrmann, G., and Spiess, V.: Quantification of gas bubble emissions from submarine hydrocarbon seeps at the Makran continental margin (offshore Pakistan), J. Geophys Res.-Oceans, 117, C10015, doi:10.1029/2011JC007424, 2012b.

Römer, M., Sahling, H., Pape, T., dos Santos Ferreira, C., Wenzhöfer, F., Boetius, A., and Bohrmann, G.: Methane fluxes and carbonate deposits at a cold seep area of the Central Nile Deep Sea Fan, Eastern Mediterranean Sea, Mar. Geol., 347, 27-42, doi:10.1016/j.margeo.2013.10.011, 2014.

Sahling, H., Bohrmann, G., Artemov, Y. G., Bahr, A., Brüning, M., Klapp, S. A., Klaucke, I., Kozlova, E., Nikolovska, A., Pape, T., Reitz, A., and Wallmann, K.: Vodyanitskii mud volcano, Sorokin trough, Black Sea: Geological characterization and quantification of gas bubble streams, Mar. Petrol. Geol., 26, 1799-1811, 2009.

Sahling, H., and cruise participants: R/V Heincke cruise report HE-387. Gas emissions at the Svalbard continental margin. Longyearbyen - Bremerhaven, 20 August - 16 September 2012., Berichte, MARUM - Zentrum für Marine Umweltwissenschaften, Fachbereich Geowissenschaften, Universität Bremen, No. 291, 170 pages, 2012.

Sarkar, S., Berndt, C., Minshull, T. A., Westbrook, G. K., Klaeschen, D., Masson, D. G., Chabert, A., and Thatcher, K. E.: Seismic evidence for shallow gas-escape features associated with a retreating gas hydrate zone offshore west Svalbard, J. Geophys. Res.-Sol Ea, 117, B09102, doi:10.1029/2011jb009126, 2012.

Sauter, E. J., Muyakshin, S. I., Charlou, J.-L., Schlüter, M., Boetius, A., Jerosch, K., Damm, E., Foucher, J.-P., and Klages, M.: Methane discharge from a deep-sea submarine mud volcano into the upper water column by gas hydrate-coated methane bubbles, Earth Planet. Sc. Lett., 243, 354-365, 2006.

Schneider von Deimling, J., Rehder, G., Greinert, J., McGinnnis, D. F., Boetius, A., and Linke, P.: Quantification of seep-related methane gas emissions at Tommeliten, North Sea, Cont. Shelf Res., 31, 867-878, 2011.

Shakova, N., Semiletov, I., Salyuk, A., Yusupov, V., Kosmach, D., and Gustafsson, Ö.: Extensive methane venting to the atmosphere from sediments of the east Siberian Arctic shelf, Science, 327, 1246-1250, doi:10.1126/science.1182221, 2010.

Solheim, A., Faleide, J. I., Andersen, E. S., ElverhØI, A., Forsberg, C. F., Vanneste, K., Uenzelmann-Neben, G., and Channell, J. E. T.: Late Cenozoic seismic stratigraphy and glacial geological development of the east Greenland and Svalbard-Barents Sea continental margins, Quaternary Sci. Rev., 17, 155-184, 1998.

Torres, M. E., McManus, J., Hammond, D., Angelis, M. A. d., Heeschen, K. U., Colbert, S. L., Tryon, M. D., Brown, K. M., and Suess, E.: Fluid and chemical fluxes in and out of sediments hosting methane hydrate deposits on Hydrate Ridge, OR, I: Hydrological provinces, Earth Planet. Sc. Lett., 201, 525-540, 2002.

Vanneste, M., Guidard, S., and Mienert, J.: Bottom-simulating reflections and geothermal gradients across the western Svalbard margin, Terra Nova, 17, 510-516, 10.1111/j.1365-3121.2005.00643.x, 2005.

Vorren, T. O., Laberg, J. S., Blaume, F., Dowdeswell, J. A., Kanyon, N. H., Mienert, J., Rumohr, J., and Werner, F.: The Norwegian-Greenland Sea continental margins: Morphology and late Quaternary sedimentary processes and environment, Quaternary Sci. Rev., 17, 273-302, 1998.

Westbrook, G. K., Chand, S., Rossi, G., Long, C., Bünz, S., Camerlenghi, A., Carcione, J. M., Dean, S., Foucher, J. P., Flueh, E., Gei, D., Haacke, R. R., Madrussani, G., Mienert, J., Minshull, T. A., Nouzé, H., Peacock, S., Reston, T. J., Vanneste, M., and Zillmer, M.: Estimation of gas hydrate concentration from multi-component seismic data at sites on the continental margins of NW Svalbard and the Storegga region of Norway, Mar. Petrol. Geol., 25, 744-758, 2008.

Westbrook, G. K., Thatcher, K. E., Rohling, E. J., Piotrowski, A. M., Pälike, H., Osborne, A. H., Nisbet, E. G., Minshull, E. A., Lanoisellé, M., James, R. H., Hühnerbach, V., Green, D., Fisher, R. E., Crocker, A. J., Chabert, A., Bolton, C., Beszczynska-Möller, A., Berndt, C., and Aquilina, A.: Escape of methane gas from the seabed along the west Spitsbergen continental margin, Geophys. Res. Lett., 36, L15608, doi:10.1029/2009GL039191, 2009.

Whiticar, M. J.: A geochemial perspective of natural gas and atmospheric methane, Org. Geoch., 16, 531-547, doi:10.1016/0146-6380(90)90068-B, 1990.

Wright, I. C.: RRS James Clark Ross Cruise 253 (26 Jul - 25 Aug 2011) Arctic methane hydrates, National Oceanography Centre, Southampton, Southampton, 2012.

Tables

Table 1. Stations and instruments deployed during R/V Heincke cruise HE-387. Abbreviations: ROV=remotely operated vehicle MARUM-Cherokee; GBS=Gas bubble sampler; Marker=seafloor deployed stone with a syntactic floating foam bound to it.

Date	Stat. No.	Stat. No. GeoB	Instrument	Latitude	Longitude	Water depth (m)
23 Aug 2012	7	16807	ROV Dive 01	ca. 78°32.9' N	ca. 10°14.2' E	91
23 Aug 2012	7-1	16807-1	Marker 2	78°32.839' N	10°14.247' E	94
23 Aug 2012	7-2	16807-2	GBS 1	78°32.839' N	10°14.252' E	94
23 Aug 2012	7-3	16807-3	GBS 2	78°32.840' N	10°14.247' E	94
24 Aug 2012	12	16812	ROV Dive 02	ca. 78°32.8' N	ca. 10°14.3' E	83
25 Aug 2012	16	16816	ROV Dive 03	ca. 78°32.8' N	ca. 10°14.2' E	94
27 Aug 2012	23	16823	ROV Dive 04	ca. 78°39.2' N	ca. 9°25.8' E	241
27 Aug 2012	23-1	16823-1	Marker 1	78°39.253' N	9°25.760' E	241
27 Aug 2012	23-2	16823-2	GBS 1	78°39.254' N	9°25.755' E	242
27 Aug 2012	23-4	16823-4	Marker 4	78°39.252' N	9°26.044' E	241
27 Aug 2012	23-5	16823-5	GBS 2	78°39.252' N	9°26.041' E	240
28 Aug 2012	26	16826	ROV Dive 05	ca. 78°39.2' N	ca. 9°26.0' E	243
30 Aug 2012	33	16833	ROV Dive 06	ca. 78°37.1' N	ca. 9°24.6' E	382
30 Aug 2012	33-1	16833-1	Marker 5	78°37.220' N	9°24.659' E	381
30 Aug 2012	33-2	16833-2	GBS 1	78°37.218' N	9°24.659' E	382
30 Aug 2012	33-3	16833-3	GBS 2	78°37.210' N	9°24.570' E	384
30 Aug 2012	33-4	16833-4	Marker 3	78°37.209' N	9°24.565' E	384
02 Sept 2012	46	16846	ROV Dive 07	ca. 78°35.4' N	ca. 9°26.5' E	386
03 Sept 2012	48	16848	ROV Dive 08	ca. 78°33.4' N	ca. 9°28.3' E	391
03 Sept 2012	48-1	16848-1	Marker 8	78°33.334' N	9°28.509' E	387
03 Sept 2012	48-2	16848-2	GBS	78°33.326' N	9°28.558' E	387
04 Sept 2012	53	16853	ROV Dive 09	ca. 78°34.5' N	ca. 10°10.2' E	90

Table 2. Proportions of low-molecular-weight alkanes and CO_2 [in mol.% of $\Sigma(C_1–C_3, CO_2)$] in vent gas samples taken with the Gas Bubble Sampler (b.d.l. = below detection limit).

Area	Depth	ROV Dive	GeoB	CH_4 (mol-%)	C_2H_6 (mol-%)	CO_2 (mol-%)	C_3H_8 (mol-%)	C_1/C_2	$\delta^{13}C$-CH_4 (‰ V-PDB)
Area 1	90 m	01	16807-2	98.977	0.013	1.009	< 0.001	7852	-43.5
Area 2	240 m	04	16823-1	99.689	0.007	0.303	< 0.001	15161	-55.8
Area 2	240 m	04	16823-3	99.730	0.007	0.261	< 0.001	13919	-55.7
Area 3	380 m	06	16833-2	99.991	0.008	b.d.l.	< 0.001	12213	-53.8
Area 3	380 m	06	16833-3	99.858	0.010	0.131	< 0.001	10325	-57.4
Area 3	380 m	08	16848-2	99.703	0.010	0.286	< 0.001	9697	-56.0

Table 3. Gas quantities transported by individual gas bubble streams in Area 2 (240 – 245 mbsl) determined by use of the gas bubble catcher or by interpretation of video footage.

Cluster	No(s). of bubble streams	ROV - Dive	Location	Tools	Stream	Flux ml /min Visual quantification	Flux ml/min Bubble catcher
C1	15	04	78°39.253’N; 9°25.760’E 241 m	Marker 1, GBS	S1	17.0	
					S2	9.9	
					S4	23.0	
C2	12	04	78°39.252’N; 9°26.044’E 241 m	Marker 4, GBS	S1	21.7	
					S2	13.0	
					S4	8.5	
					S5	6.6	
					S6	20.5	
C3	1	05	78°39.216’N; 9°25.834’E 242 m		S1	26.5	27.9
C4	1	05	78°39.216’N; 9°25.786’E 241 m		S1	5.2	4.0
C5	1	05	78°39.228’N; 9°25.735’E 242 m				
C6	5	05	78°39.201’N; 9°25.995’E 241 m		S1		25.0
					S2		19.4
					S3		6.2
					S4		8.2
					S5		17.1

Table 4. Estimated number of flares in Area 3 following the approach described in the text and illustrated in Fig. 9.

Profile	Observed area	Number of flares in observed area	Ratio observed area to ‘seep area’ (3.72 km²) in %	Estimated total number of flares in ‘seep area’
Fig. 9 A	2.35 km²	294	63.1	466
Fig. 9 B	2.89 km²	407	77.7	524
Fig. 9 C	2.88 km²	334	77.4	432
Fig. 9 D	2.38 km²	246	64.0	384
Average				451.5

Table 5. Gas quantities transported by of individual gas bubble streams in Area 3 (‘396-m flares’) determined by use of the gas bubble catcher and by interpretation of video footage.

Cluster	Number of bubble streams	Dive	Location Depth	Tools	Stream	Flux ml /min Visual quantification	Flux ml/min Bubble catcher
C1	10	06	78°37.220’N; 9°24.659’E, 385 m	Marker 5, GBS 1	S1	9.4	
C3	3	06	78°37.209’N; 9°24.565’E; 385 m	Marker 3, GBS 2	S1	6.7	
C5	8	07	78°35.380’N; 9°26.627’E; 385 m		S1		6.3
					S2		31.0
					S3		37.5
					S4		41.0
C6	8	07	78°35.381’N; 9°26.604’E; 385 m		S1		3.0
					S2		32.0
C7	4	07	78°35.380’N; 9°26.831’E; 386 m				
C8	5	07	78°33.335’N; 9°28.527’E; 385 m	Marker 8			
C9	6	07	78°33.326’N; 9°28.548’E; 385 m				
C10	3	07	78°33.310’N; 9°28.647’E; 385 m				
C11	6	07	78°33.299’N; 9°28.603’E; 389 m				

Table 6. Fluxes of bubble-forming methane from the seafloor to the hydrosphere in various regions.

Methane bubble flux (10^6 mol yr^{-1})	Water depth (m)	Area	Reference
27 (5 to 68)	240 – 245	Area 2	This study
26 (4 to 50)	380 – 390	Area 3	This study
~19	1250 – 1270	Håkon Mosby Mud Volcano - all three emission sites	Sauter et al., 2006
2 to 87	890	Kerch Flare, Black Sea	Römer et al., 2012a
21.9	600 – 700	Northern summit Hydrate Ridge, offshore Oregon	Torres et al., 2002
1.5	65 – 75	Tommeliten field, North Sea	Schneider von Deimling et al., 2011
40 (±32)	575 – 2870	Makran continental margin (50 km broad segment)	Römer et al., 2012b
0.23 to 2.3	1690	Carbonate slab, Nile Deep Sea Fan	Römer et al., 2014

Table 7. Amount of methane either released as bubbles from the seafloor (this study) or susceptible to temperature-induced hydrate dissociation as revealed from modeling.

Description	Amount methane (10^6 mol yr^{-1})	Margin width (km)	Amount methane (10^3 mol yr^{-1} m^{-1})	Reference
Methane flux as bubbles (Area 2)	27 (5 to 68)	4.5	6.0 (1.1 to 15.1)	This study
Methane flux as bubbles (Area 3)	26 (4 to 50)	11	2.4 (0.4 to 4.5)	This study
Methane flux as bubbles (Area 2 & 3)	53 (9 to 118)	~14	3.8 (0.6 to 8.4)	This study
Progressive dissociation of hydrate	1683	30	56.1	Westbrook et al., 2009
Progressive dissociation of hydrate	264	30	8.8	Reagan et al., 2011
Future (100 years) dissociation of hydrates	171 to 514	25	6.9 to 20.6	Marín-Moreno et al., 2013
Future (300 years) dissociation of hydrates	330 to 1807	25	13.2 to 72.3	Marín-Moreno et al., 2013
Annual hydrate formation and dissociation			561 to 935	Berndt et al., 2014

Figure captions

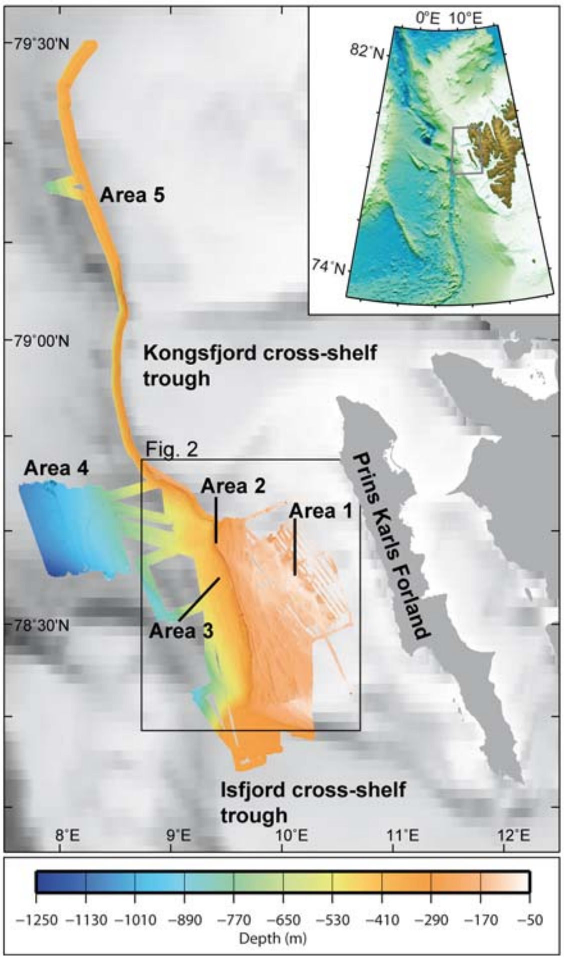

Figure 1. Multibeam bathymetry obtained during R/V Heincke cruise 387 (colour) plotted on IBACO bathymetry (Jakobsson et al., 2008) showing the study areas (Areas 1 to 5) at the continental margin west of Svalbard. Inset shows an overview map with the location of the main map.

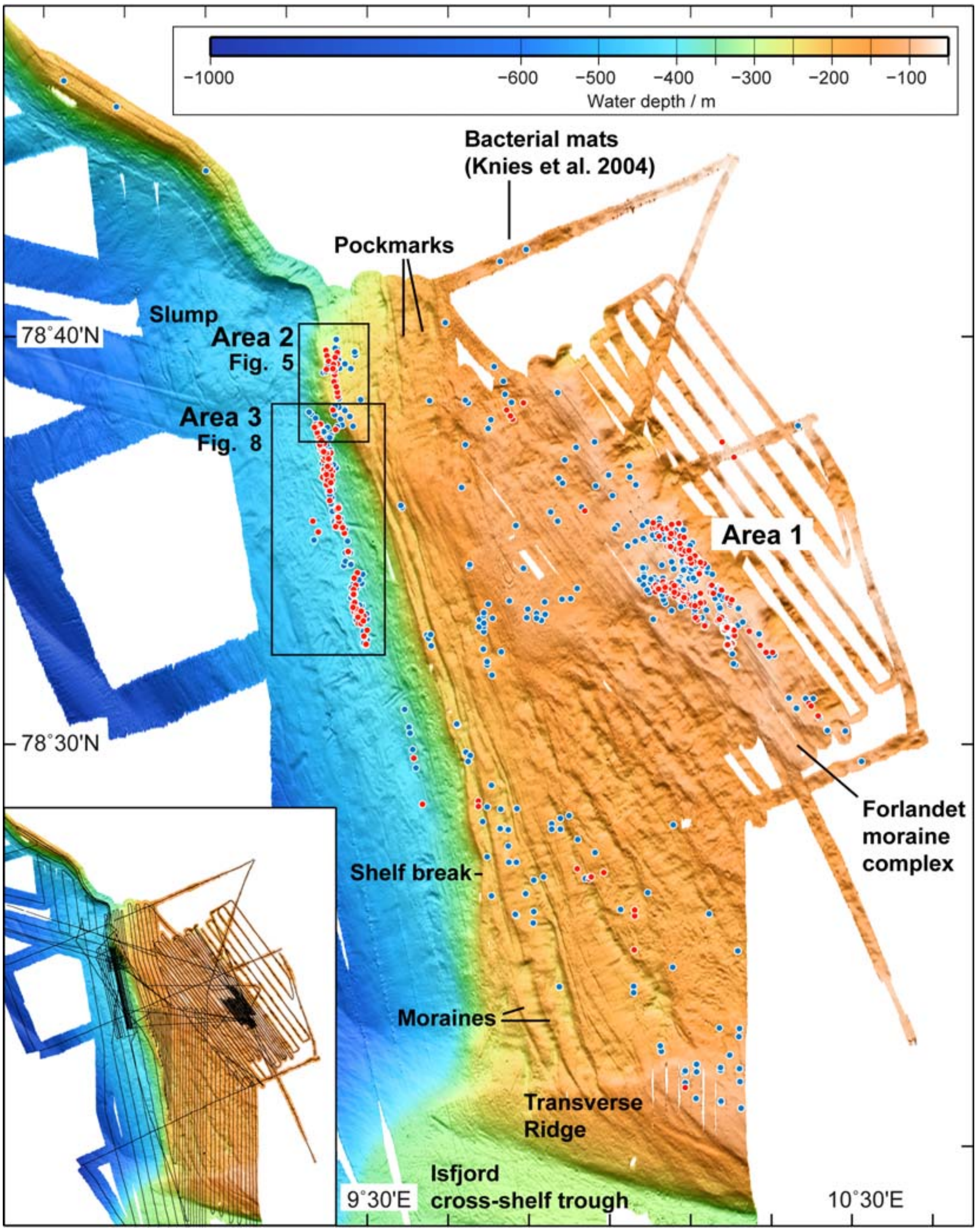

Figure 2. Main figure: Location of flares (hydroacoustic indications of gas bubble emissions) during summer 2012 as picked from EK 60 echosounder records plotted on top of multibeam bathymetry. Strong flares (red dots) mainly occur in Areas 1, 2, and 3. Weak flares (blue dots) occur widespread at the shelf. Inset: Map of that region showing the ship track and bathymetry.

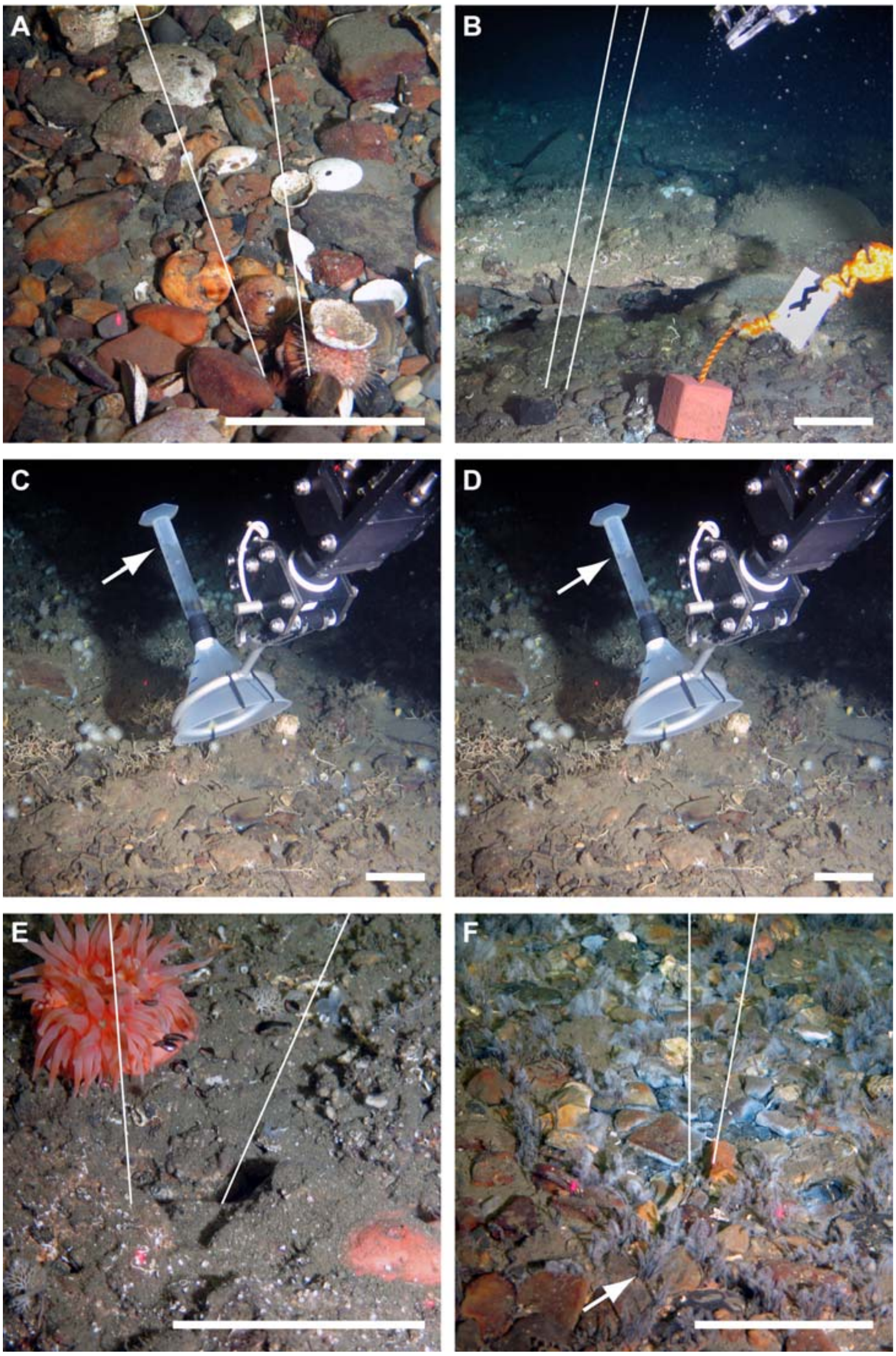

Figure 3. Seafloor images taken during dives with ROV at gas emission sites in Area 1 (A), Area 2 (B-E), and Area 3 (F). Scale bar is 10 cm. Arrows point to objects of interest, white lines outline the trace of the rising bubbles. (A) Bubbles escaping from the cobble-covered seafloor (Dive 02). (B) Three bubble streams at Marker 4. Crusts resembling authigenic carbonates at the seafloor (Dive 04). (C), (D) Images illustrating the use of the bubble catcher for measuring the gas bubble volume flux (Dive 05). (E) Bubbles rising in front of an anemone (Dive 04). (F) Filamentous (probably sulfur-oxidizing) bacteria and pogonophora at a bubble stream (Dive 08). Photos courtesy of MARUM.

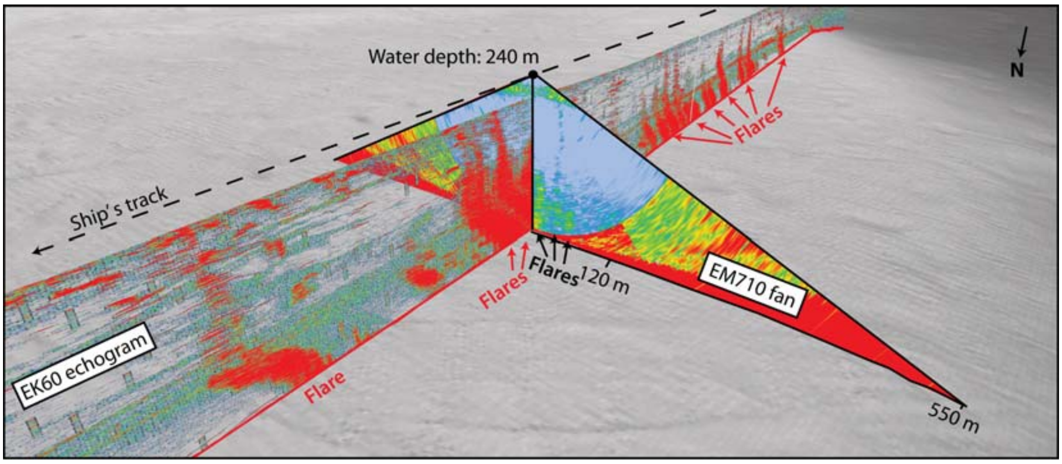

Figure 4. Composite figure illustrating the appearance of flares in single beam EK 60 echosounder and in multibeam EM 710 echosounder. Flares can be traced in the central part of the EM 710 fan (45° to each side), in this example obtained in 240 m water depth, the across track width is 120 m to each side. Beyond that limit, the noise is too high to reliably map flares.

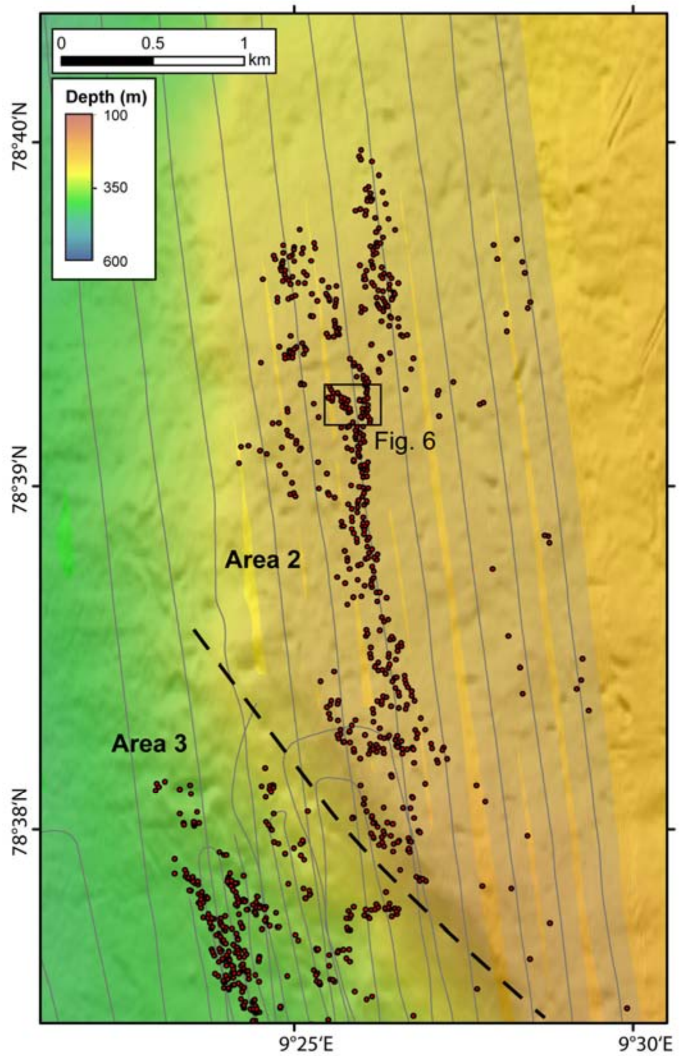

Figure 5. Flares (circles) in Area 2 (240 to 245 mbsl) plotted on shaded bathymetry. Flares were picked in multibeam water column data; the coverage is shown as grey shading around the ship track (lines). ROV dives were performed in an area highlighted by the rectangular box (Fig. 6).

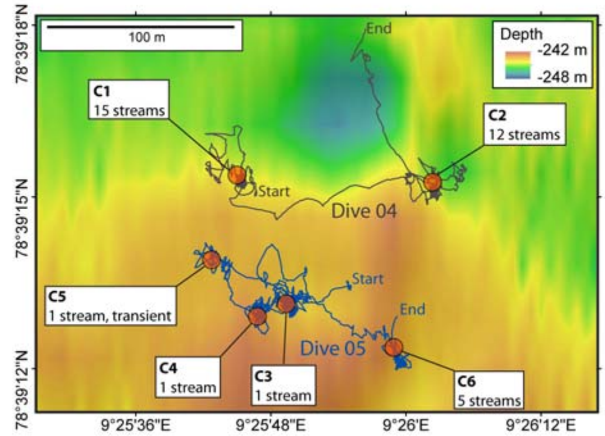

Figure 6. Bubble stream clusters (C1 to C6) in Area 2 discovered during ROV dives 04 and 05. Dive tracks are shown on bathymetry.

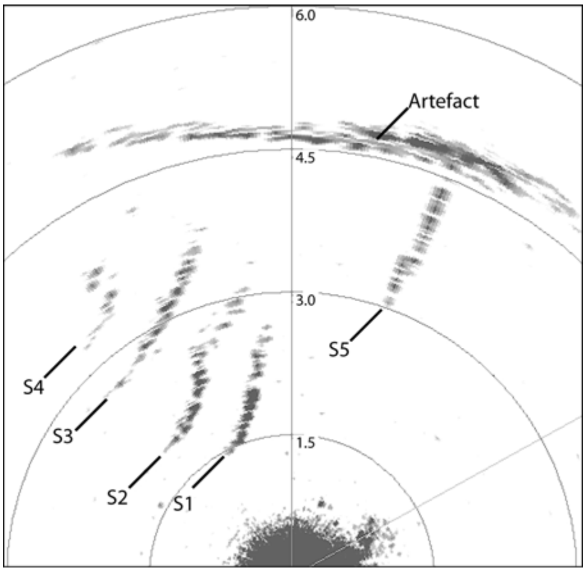

Figure 7. Screenshot of the record from the horizontally-looking sonar (Sonar Tritech, 625 kHz, 6 m range) mounted on the ROV (Dive 05, 14:37:27 UTC). The image shows the five bubble streams S1 to S5 at cluster C5 at the western edge of the dive track.

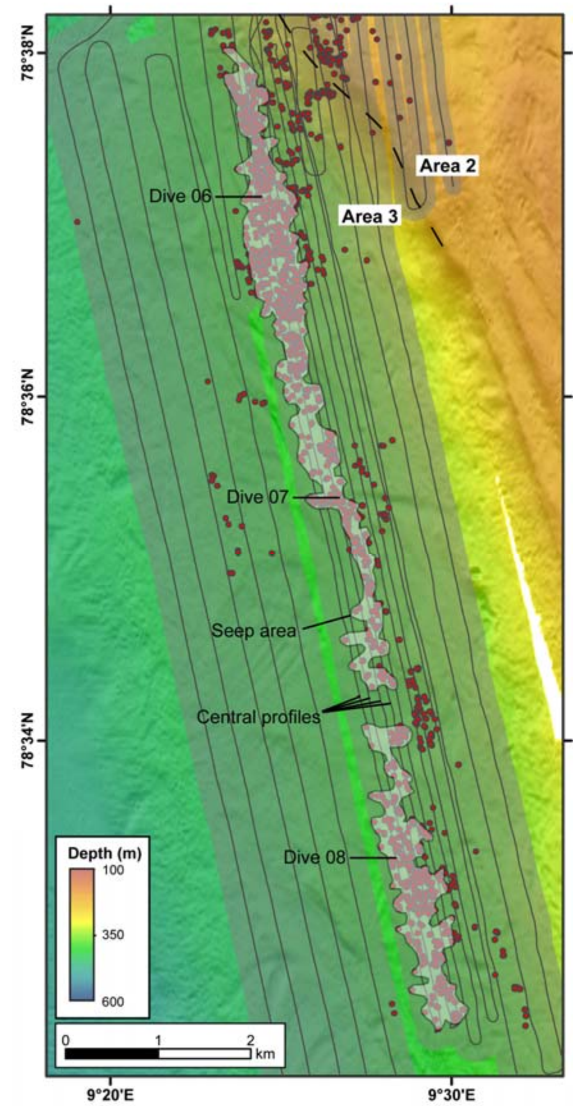

Figure 8. Position of flares (circles) found in Area 3 ('396-m flares') plotted on shaded bathymetry. Flares were picked in multibeam water column data; the coverage is shown as dark grey shading around the ship track (lines). In this study we defined a 'seep area' (light grey shading) in which the number of flares was quantified using the four central profiles (see Figure 9). The approximate locations where the three ROV dives (06-08) are indicated.

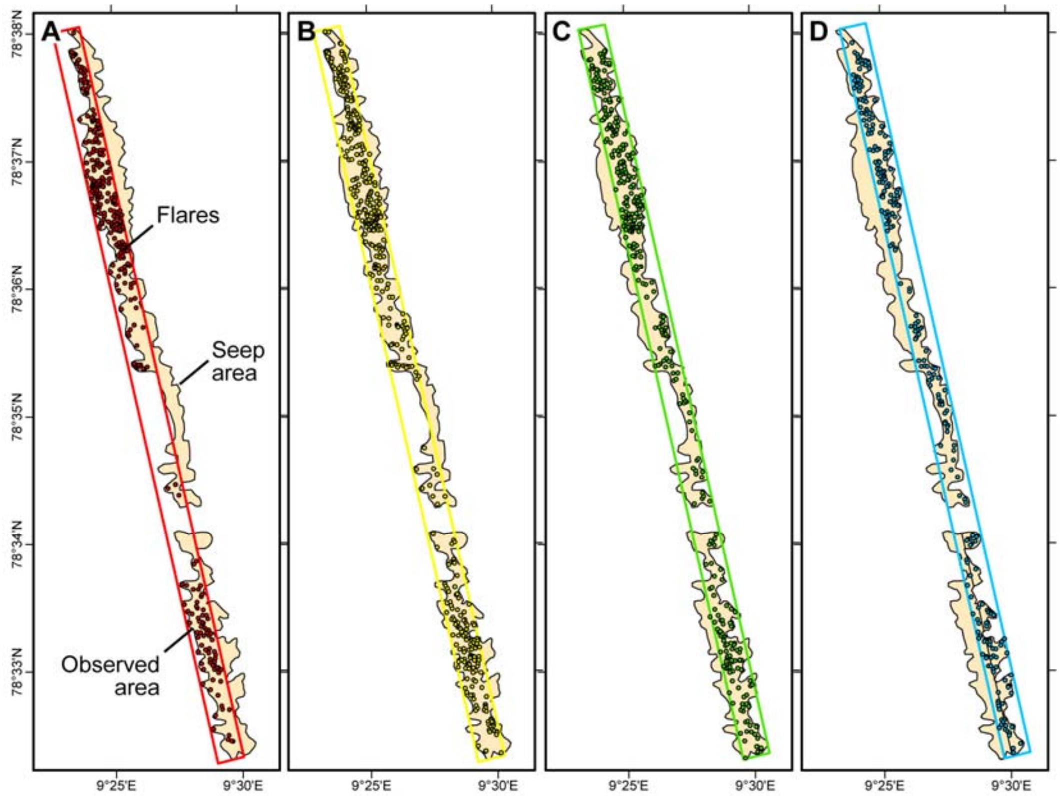

Figure 9. Diagram illustrating the approach of quantifying flares in Area 3. Numbers of flares were estimated within the 'observed area', which is the region covered by multibeam (rectangular box) intersecting with the 'seep area'. Occurrence of flares were repeatedly determined along four parallel profiles (A-D) as indicated in Figure 8 and summarized in Table 4.

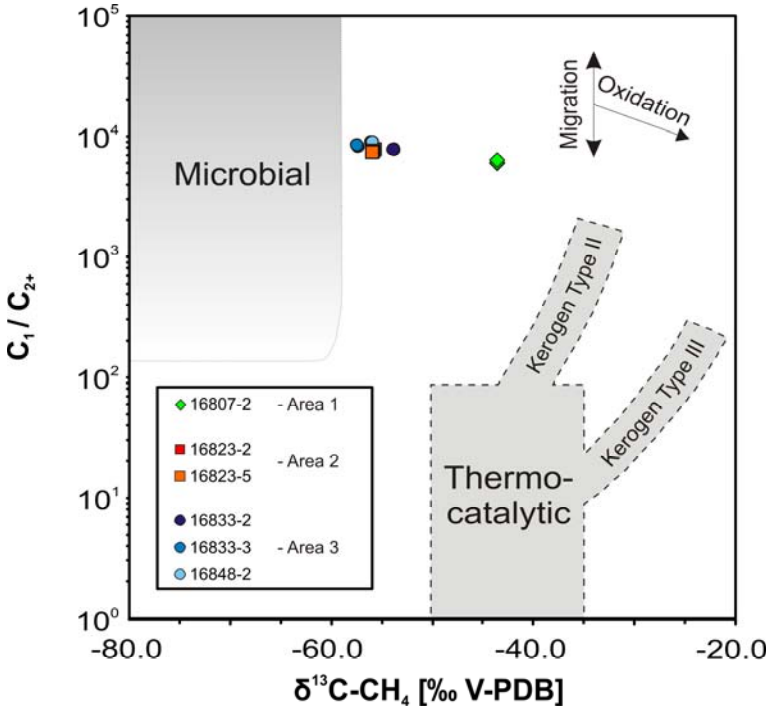

Figure 10. Molecular (C_1/C_{2+}) vs. stable C isotopic composition of methane ($\delta^{13}C$-CH_4) sampled in Areas 1–3. Classification according to the 'Bernard diagram' modified after Whiticar (1990). Gas samples studied herein plot to close to the empirical field of microbial methane except for those from Area 1.

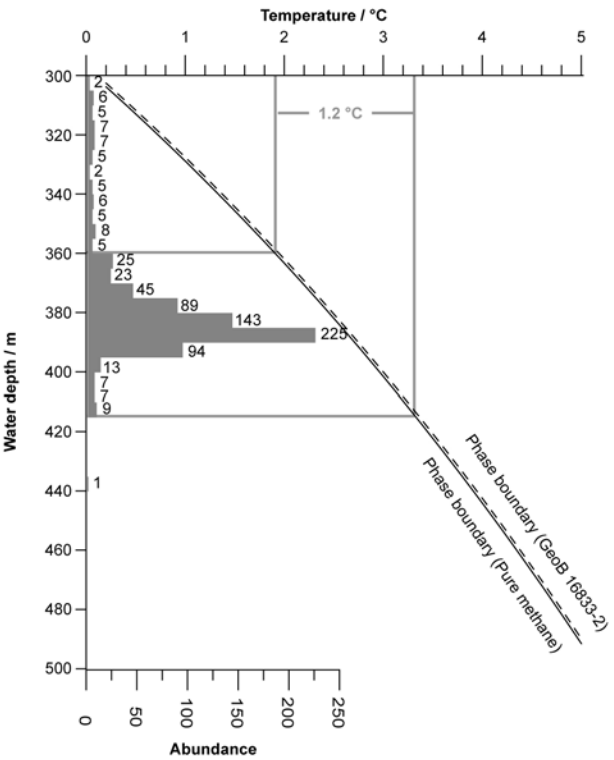

Figure 11. Composite figure showing the hydrate (structure I) phase boundary and the abundance of flares in Area 3 in 5m-depth intervals. Phase boundaries were calculated considering bottom water salinity and the molecular composition of (i) gas sample GeoB 16833-2 collected with the Gas Bubble Sampler in Area 3 (Table 2) and (ii) pure methane.